The Astrophysical Journal, 631:231–243, 2005 September 20

OXYGEN ABUNDANCE DETERMINATION IN H II REGIONS: THE STRONG LINE INTENSITIES–ABUNDANCE CALIBRATION REVISITED

Leonid S. Pilyugin
Main Astronomical Observatory of National Academy of Sciences of Ukraine, 27 Zabolotnogo Street, 03680 Kiev, Ukraine; pilyugin@mao.kiev.ua

and

Trinh X. Thuan
Astronomy Department, University of Virginia, P.O. Box 3818, University Station, Charlottesville, VA 22903; txt@virginia.edu
Received 2004 December 1; accepted 2005 May 29

ABSTRACT

The problem of oxygen abundance determination in H II regions based on the "strong oxygen line intensities–oxygen abundance" empirical calibration is revisited. A compilation of spectroscopic data of H II regions in spiral and irregular galaxies with a measured [O III] λ4363 line intensity has been carried out, resulting in a sample containing more than 700 individual measurements. Methods are devised to select out only high-precision measurements from that original sample. T_e-based oxygen abundances have been recomputed in the same way for all H II regions with high-precision measurements. That sample of T_e abundances is used to recalibrate the empirical relations between the oxygen abundance and the strong oxygen line intensities for both high (the upper branch of the O/H-R_{23} diagram) and low (the lower branch) metallicities, within the framework of the P method, where P is the excitation parameter. Concerning high-metallicity H II regions, an alternative way for deriving oxygen abundances using only measurements of the strong nebular oxygen lines is proposed. The method is based on a tight correlation between the flux in the auroral [O III] λ4363 line and the fluxes in the nebular [O II] $\lambda\lambda$3727, 3729 and [O III] $\lambda\lambda$4959, 5007 lines, called the ff relation. This relation is also used to select out high-metallicity H II regions with high-precision $(\mathrm{O/H})_{T_e}$ measurements. In contrast to previous work, the new upper branch P calibration is based only on $(\mathrm{O/H})_{T_e}$ abundances. It is found that $(\mathrm{O/H})_P$ abundances usually agree well with the $(\mathrm{O/H})_{\mathrm{ff}}$ abundances, although faint ($\log R_{23} \lesssim -0.5$) low-excitation ($P \lesssim 0.25$) H II regions may show systematic differences that can be as large as $\sim$0.1 dex. As for the newly derived low-metallicity P calibration, it is shown to be robust. The calibrations derived from the sample containing all $(\mathrm{O/H})_{T_e}$ abundance determinations and from that containing only recent (since 1995) measurements are found to be in very good agreement. For both low- and high-metallicity H II regions, the new calibration gives $(\mathrm{O/H})_P$ abundances that agree with $(\mathrm{O/H})_{T_e}$ abundances to within 0.1 dex.

Subject headings: galaxies: abundances — H II regions — ISM: abundances

1. INTRODUCTION

Spectrophotometric observations of H II regions exist now for a large number of spiral and irregular galaxies, allowing for the derivation of their heavy element content. The precision of these abundance determinations depends in large part on the method employed. Accurate abundances in H II regions can be derived from measurements of temperature-sensitive line ratios, such as [O III] $\lambda\lambda$4959, 5007/[O III] λ4363. This is often referred to as the T_e method, T_e being the electron temperature of the H II region. Unfortunately, in low-excitation oxygen-rich H II regions, temperature-sensitive lines such as [O III] λ4363 are often too weak to be detected. For such H II regions, one has to resort to abundance indicators based on more readily observable lines. Such methods have been proposed by Pagel et al. (1979) and Alloin et al. (1979). The oxygen abundance indicator $R_{23} = ([\mathrm{O\ II}]\ \lambda\lambda 3727,\ 3729 + [\mathrm{O\ III}]\ \lambda\lambda 4959,\ 5007)/\mathrm{H}\beta$ suggested by Pagel et al. (1979) has found widespread acceptance and use. Grids of photoionization models have been used to calibrate the relation between the line intensities of easily observable strong oxygen lines and the oxygen abundance (e.g., Edmunds & Pagel 1984; McCall et al. 1985; Dopita & Evans 1986; Kobulnicky et al. 1999; Kewley & Dopita 2002). However, different models by different authors give divergent calibrations, so it is best to base the calibration on oxygen abundances derived through the T_e method (Pilyugin 2003b). The strategy is very simple: the relation between the line intensities of easily observable strong oxygen lines and the oxygen abundance is calibrated using H II regions for which oxygen abundances have been determined accurately through the T_e method, and this relation is then used for abundance determination in H II regions for which the temperature-sensitive lines are not available.

The earliest calibrations were one-dimensional (Edmunds & Pagel 1984; McCall et al. 1985; Dopita & Evans 1986; Zaritsky et al. 1994), i.e., they had the functional form $\mathrm{O/H} = f(R_{23})$, where O/H depends on the unique parameter R_{23}. It has been argued (Pilyugin 2000, 2001a, 2001b) that oxygen abundances derived with such a one-dimensional calibration are systematically in error. Indeed, the intensities of the oxygen emission lines generally do not depend only on the oxygen abundance of the H II region but also on its physical conditions, as characterized, for example, by the hardness of its ionizing radiation or its geometry. These physical conditions are taken directly into account in the T_e method through the very use of T_e, but they are ignored in one-dimensional calibrations. Following the suggestion of McGaugh (1991) that the strong oxygen lines may contain the necessary information to determine the oxygen abundance in low-metallicity H II regions, Pilyugin (2000, 2001a, 2001b) has shown that the physical conditions in an H II region can be estimated and taken into account via the excitation parameter P. He proposed a more general two-dimensional parametric calibration of the functional form $\mathrm{O/H} = f(P,\ R_{23})$ called the P method.

Within the framework of the P method, the strong oxygen line intensities versus oxygen abundance calibrations have been derived both at low (Pilyugin 2000) and high (Pilyugin 2001a) O/H.

In this paper, we look at these calibrations anew for both high- and low-metallicity objects. There are several reasons that motivate us to update the high-metallicity calibration. First, the earlier calibration was based on a limited sample of ~40 H II regions. Here we have searched the literature to assemble a sample more than 1 order of magnitude larger than the previous sample. Second, the H II regions with T_e-based abundances in the earlier sample all have high or moderate excitation, with the excitation parameter $P \gtrsim 0.4$. To extend the calibration to lower values of P, a supplementary sample of low-excitation H II regions, with R_G-based oxygen abundances estimated from the "oxygen abundance–galactocentric distance" relation, was used. Recently, Bresolin et al. (2004) used the auroral lines [S III] λ6312 and [N II] λ5755 to determine T_e-based abundances in 10 low-excitation H II regions in the spiral galaxy M51. This allows us to derive an empirical calibration based on $(\mathrm{O/H})_{T_e}$ abundances over the entire range of P. Third, individual T_e-based abundance measurements in high-metallicity H II regions can have large uncertainties. The recently discovered tight empirical correlation between the auroral and nebular oxygen line fluxes in spectra of H II regions (the flux-flux, or ff, relation [Pilyugin 2005]) permits to select only those measurements that are accurate, thus putting the high-metallicity calibration on a firmer ground.

There are also reasons to update the low-metallicity calibration. First, as is the case for the high-metallicity sample, by searching the literature we can considerably augment the calibrating sample from the original number of ~40 H II regions. Second, the somewhat rough approximation used in the previous calibration, that low-metallicity H II regions with the same values of P lie on a straight line in the O/H-R_{23} diagram, i.e., that O/H varies linearly with R_{23}, can be relaxed. Third, original abundances from various authors were used in the previous calibration, introducing some heterogeneity. We can obtain a more homogeneous data set by rederiving all abundances in the same way from the published oxygen line intensities. And finally, we can put the T_e-derived oxygen abundances on which are based the high- and low-metallicity calibrations on the same abundance scale, which was not the case before.

We describe the observational data and the sets of equations that were used to determine the oxygen abundances in the H II regions in § 2. The criterion for the selection of high-precision abundance measurements in high-metallicity H II regions is given in § 3. We discuss the oxygen strong line intensities–abundance calibration for the high-metallicity upper branch of the O/H-R_{23} diagram in § 4. Section 5 gives the corresponding calibration for the low-metallicity lower branch of the O/H-R_{23} diagram. We discuss the reliability of our calibrations in § 6 and summarize our conclusions in § 7.

We use the following notations throughout the paper: $R_2 = I_{[\mathrm{O\,II}]\lambda3727+\lambda3729}/I_{\mathrm{H}\beta}$, $R_3 = I_{[\mathrm{O\,III}]\lambda4959+\lambda5007}/I_{\mathrm{H}\beta}$, $R = I_{[\mathrm{O\,III}]\lambda4363}/I_{\mathrm{H}\beta}$, $R_{23} = R_2 + R_3$, and $X_{23} = \log R_{23}$. On the basis of these definitions, the excitation parameter P can be expressed as $P = R_3/(R_2 + R_3)$.

2. THE O/H-R_{23} DIAGRAM

2.1. *Observational Data: Line Intensities*

We have carried out an extensive search of the literature to compile a list of more than 700 individual spectra of H II regions in irregular and spiral galaxies, with the requirement that they all possess a detected [O III] λ4363 emission line. While we have tried to include as many sources as possible, we do not claim our search to be exhaustive. We discuss how to select out only high-quality data from the sample for high-metallicity objects in § 3 and for low-metallicity objects in § 5.

For each spectrum, we record the measured values of R_2, R_3, and R. When several measurements of the same H II region are available, we include all of them, treating them as independent measurements. These do not exceed five for a single H II region. When the $I_{[\mathrm{O\,III}]\lambda4959}$ line intensity is not available, the value of R_3 is obtained from the relation $R_3 = 1.346 \times I_{[\mathrm{O\,III}]\lambda5007}/I_{\mathrm{H}\beta}$. The sources of the spectra are listed in Table 1, where we have also given the number of spectra taken from each source. The spectroscopic data so assembled form the basis of the present study.

2.2. *Abundance Derivation*

In principle, the T_e method based on the measurement of temperature-sensitive line ratios such as [O III] ($\lambda\lambda$4959, 5007)/λ4363 can give accurate oxygen abundances. In practice, however, oxygen abundances in the same H II region derived by various authors can differ for three basic reasons: (1) there are errors in the line intensity measurements, (2) the adopted atomic data are not the same, and (3) the adopted model for the electron temperature structure differs. For example, it can be a one-zone model with a single characteristic T_e, a two-zone model with two T_e-values, or a model with small-scale temperature fluctuations. Therefore, to ensure that we have a relatively homogeneous data set, we decided not to use the original T_e-based oxygen abundance determinations carried out over a time span of more than 25 years but to calculate them ourselves in the same way for all H II regions with a measured [O III] ($\lambda\lambda$4959, 5007)/λ4363 line ratio.

We adopt a two-zone model for the temperature structure within a H II region. Pagel et al. (1992) have published a set of equations for the determination of the oxygen abundance in H II regions. According to those authors, the electron temperature t_3 within the [O III] zone, in units of 10^4 K, is given by the following equation:

$$t_3 = \frac{1.432}{\log(R_3/R) - 0.85 + 0.03\log t_3 + w}, \tag{1}$$

where

$$w = \log\left(1 + 0.0433 x_2 t_3^{0.06}\right) \tag{2}$$

and

$$x_2 = 10^{-4} n_e t_2^{-1/2}. \tag{3}$$

Here n_e is the electron density in cm^{-3} and t_2 is the electron temperature within the [O II] zone.

The oxygen abundances are then derived from the following equations:

$$\frac{\mathrm{O}}{\mathrm{H}} = \frac{\mathrm{O}^+}{\mathrm{H}^+} + \frac{\mathrm{O}^{++}}{\mathrm{H}^+}, \tag{4}$$

$$12 + \log\left(\frac{\mathrm{O}^{++}}{\mathrm{H}^+}\right) = \log R_3 + 6.174 + \frac{1.251}{t_3} - 0.55\log t_3, \tag{5}$$

$$12 + \log\left(\frac{\mathrm{O}^{+}}{\mathrm{H}^+}\right) = \log R_2 + 5.890 + \frac{1.676}{t_2} - 0.40\log t_2 + \log(1 + 1.35 x_2). \tag{6}$$

TABLE 1
References to Spectroscopic Data

Reference	n[a]	Reference	n[a]	Reference	n[a]
Augarde et al. (1990)	1	Izotov & Thuan (2004)	32	Peimbert (1967)	5
Axon et al. (1988)	2	Izotov et al. (1991)	5	Peimbert & Torres-Peimbert (1974)	6
Baldwin et al. (2000)	1	Izotov et al. (1994)	9	Peimbert & Torres-Peimbert (1976)	4
Bergvall (1985)	1	Izotov et al. (1996)	5	Peimbert & Torres-Peimbert (1992)	1
Bergvall & Östlin (2002)	4	Izotov et al. (1997)	25	Peimbert et al. (1993)	1
Campbell et al. (1986)	30	Izotov et al. (1999)	7	Peimbert et al. (2000)	15
Caplan et al. (2000)	6	Izotov et al. (2001a)	2	Popescu & Hopp (2000)	23
de Blok & van der Hulst (1998)	2	Izotov et al. (2001b)	1	Pustilnik et al. (2002)	2
de Naray et al. (2004)	4	Izotov et al. (2004)	9	Pustilnik et al. (2003a)	1
Díaz et al. (1987)	3	Kennicutt & Skillman (2001)	1	Pustilnik et al. (2003b)	3
Dinerstein & Shields (1986)	1	Kennicutt et al. (2003)	17	Pustilnik et al. (2004)	2
Dufour (1975)	14	Kinman & Davidson (1981)	9	Rayo et al. (1982)	2
Dufour & Harlow (1977)	12	Kniazev et al. (2003)	2	Rego et al. (1998)	1
Durret et al. (1985)	1	Kobulnicky & Skillman (1996)	2	Rönnback & Bergvall (1995)	14
Edmunds & Pagel (1984)	3	Kobulnicky & Skillman (1997)	4	Rosa & Mathis (1987)	9
Esteban et al. (1998)	2	Kobulnicky & Skillman (1998)	5	Shaver et al. (1983)	2
Esteban et al. (1999a)	2	Kobulnicky et al. (1997)	3	Shields & Searle (1978)	2
Esteban et al. (1999b)	1	Kunth & Joubert (1985)	28	Skillman (1985)	3
Esteban et al. (2004)	1	Kunth & Sargent (1983)	13	Skillman & Kennicutt (1993)	2
Fierro et al. (1986)	1	Kurt et al. (1999)	4	Skillman et al. (1989a)	4
French (1980)	10	Kwitter & Aller (1981)	5	Skillman et al. (1989b)	2
Fricke et al. (2001)	1	Lee et al. (2003a)	11	Skillman et al. (1994)	3
García-Rojas et al. (2004)	1	Lee et al. (2003b)	1	Skillman et al. (2003)	6
Garnett & Kennicutt (1994)	1	Lee et al. (2005)	4	Smith (1975)	9
Garnett et al. (1997)	5	Lequeux et al. (1979)	6	Terlevich et al. (1991)	58
Garnett et al. (1999)	1	Luridiana et al. (2002)	2	Thuan et al. (1995)	5
Gonzalez-Delgado et al. (1994)	14	McCall et al. (1985)	8	Thuan et al. (1999)	3
Gonzalez-Riestra et al. (1987)	1	McGaugh (1994)	5	Torres-Peimbert et al. (1989)	3
Gonzalez-Riestra et al. (1988)	1	Melbourne et al. (2004)	12	Tsamis et al. (2003)	5
Guseva et al. (2000)	3	Melnick et al. (1992)	2	Tully et al. (1981)	2
Guseva et al. (2001)	2	Miller (1996)	3	van Zee (2000)	2
Guseva et al. (2003a)	2	Miller & Hodge (1996)	1	van Zee et al. (1997)	17
Guseva et al. (2003b)	2	Moles et al. (1990)	3	van Zee et al. (1998)	16
Guseva et al. (2003c)	2	Noeske et al. (2000)	3	Vermeij et al. (2002)	8
Guseva et al. (2004)	2	O'Connell et al. (1978)	1	Vílchez & Iglesias-Páramo (1998)	1
Heydari-Malayeri et al. (1990)	2	Oey & Shields (2000)	1	Vílchez & Iglesias-Páramo (2003)	5
Hidalgo-Gámez et al. (2001a)	5	Osterbrock et al. (1992)	1	Vílchez et al. (1988)	1
Hidalgo-Gámez et al. (2001b)	2	Pagel et al. (1979)	1	Webster & Smith (1983)	9
Hodge & Miller (1995)	4	Pagel et al. (1980)	5	Webster et al. (1983)	6
Izotov & Thuan (1998a)	2	Pagel et al. (1992)	13	Zasov et al. (2000)	2
Izotov & Thuan (1998b)	17	Peimbert (2003)	1		

[a] Number of spectra taken from this source.

Recently, a new set of equations has been proposed by Izotov et al. (2005) using the latest atomic data. In this new set of equations, the electron temperature t_3 is given by

$$t_3 = \frac{1.432}{\log(R_3/R) - \log C_T}, \tag{7}$$

where

$$C_T = \left(8.44 - 1.09t_3 + 0.5t_3^2 - 0.08t_3^3\right)v, \tag{8}$$

$$v = \frac{1 + 0.0004x_3}{1 + 0.044x_3}, \tag{9}$$

and

$$x_3 = 10^{-4} n_e t_3^{-1/2}. \tag{10}$$

As for the oxygen abundances, they are derived from the following equations:

$$12 + \log\left(\frac{O^{++}}{H^+}\right) = \log R_3 + 6.200 + \frac{1.251}{t_3} - 0.55\log t_3 - 0.014t_3, \tag{11}$$

$$12 + \log\left(\frac{O^{+}}{H^+}\right) = \log R_2 + 5.961 + \frac{1.676}{t_2} - 0.40\log t_2 - 0.034t_2 + \log(1 + 1.35x_2). \tag{12}$$

In Figure 1 (*top*), we compare for our sample of H II regions the electron temperatures $t_3(05)$ derived from equation (7) (Izotov et al. 2005) with the electron temperatures $t_3(92)$ derived from equation (1) (Pagel et al. 1992). We have adopted a constant electron density of $n_e = 100$ cm^{-3} for all H II regions. Inspection of Figure 1 (*top*) shows that $t_3(05)$ is systematically

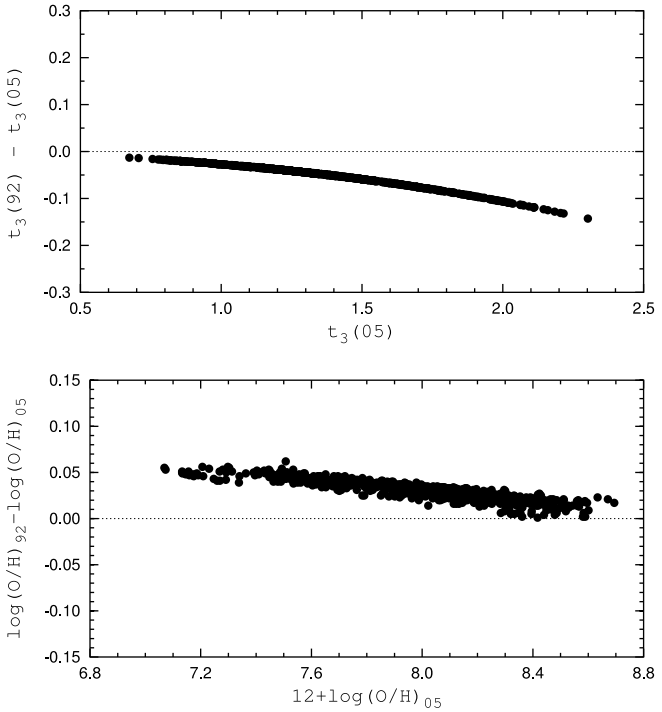

FIG. 1.—*Top*: Differences between electron temperatures $t_3(92)$ within the [O III] zone derived from eq. (1) (Pagel et al. 1992) and electron temperatures $t_3(05)$ within the [O III] zone derived from eq. (7) (Izotov et al. 2005) vs. electron temperatures $t_3(05)$ for our total sample of H II regions. *Bottom*: Differences between oxygen abundances $(O/H)_{92}$ derived from the equations of Pagel et al. (1992) and Garnett (1992) and oxygen abundances $(O/H)_{05}$ derived from the equations of Izotov et al. (2005) and Garnett (1992) vs. oxygen abundances $(O/H)_{05}$ for our total sample of H II regions.

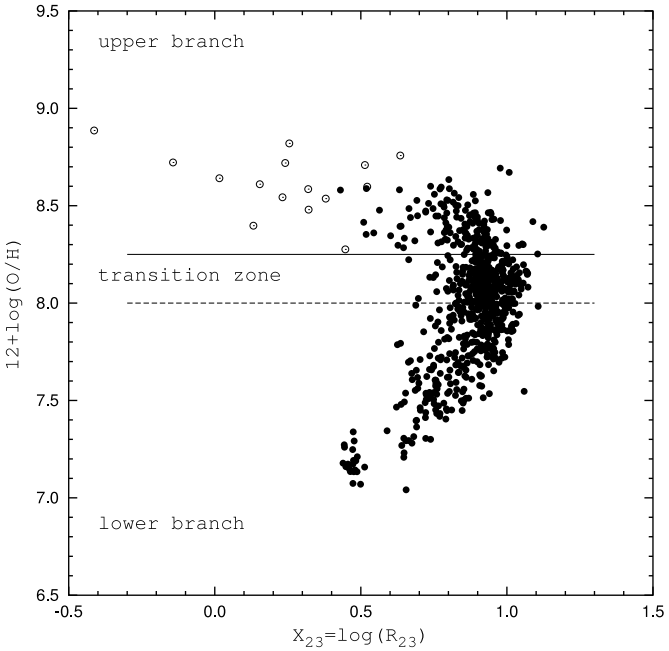

FIG. 2.—R_{23}-O/H diagram. Filled circles are H II regions from our total sample listed in Table 1, and open circles are low-excitation H II regions from Bresolin et al. (2004); Kennicutt et al. (2003); Castellanos et al. (2002). Horizontal lines show the adopted boundaries between the lower branch and the transition zone (*dashed line*) and between the upper branch and the transition zone (*solid line*).

higher than $t_3(92)$. The difference is small at low temperatures but increases toward high temperatures, reaching about 0.1 at $t_3(05) = 2$.

The electron temperature t_2 of the [O II] zone is usually determined from an equation that relates t_2 to t_3, derived by fitting H II region models. Several versions of this t_2-t_3 relation have been proposed (e.g., Garnett 1992; Pagel et al. 1992; Izotov et al. 2005). We have adopted the Garnett relation (Garnett 1992),

$$t_2 = 0.7t_3 + 0.3, \quad (13)$$

because there is observational evidence in support of it at both low and high metallicities (see the discussion in Bresolin et al. 2004).

In Figure 1 (*bottom*) we compare the oxygen abundances $(O/H)_{05}$ derived from the Izotov et al. (2005) plus Garnett (1992) equations with the oxygen abundances $(O/H)_{92}$ derived from the Pagel et al. (1992) plus Garnett (1992) equations for our sample of H II regions. Inspection of Figure 1 (*bottom*) shows that $(O/H)_{92}$ is systematically higher than $(O/H)_{05}$, with the difference $\Delta\log(O/H) = \log(O/H)_{92} - \log(O/H)_{05}$ decreasing with increasing metallicity. However, the two sets of abundances can be considered to be in relative good agreement, since the largest differences do not exceed 0.06 dex. We thus adopt the equations of Izotov et al. (2005) and Garnett (1992) (eqs. [4], [7]–[13]) to determine oxygen abundances. These are referred to hereafter as T_e-based oxygen abundances.

2.3. *The* O/H-R_{23} *Diagram*

Figure 2 shows the R_{23}-O/H diagram for our H II region sample (*filled circles*). We have also plotted (*open circles*) the data on 10 low-excitation H II regions in the spiral galaxy M51, in which Bresolin et al. (2004) have detected the auroral lines [S III] λ6312 and/or [N II] λ5755. These lines allow them to measure T_e and derive accurate oxygen abundances. To reduce the original abundances to our abundance scale, we have recomputed them using t_3 and t_2 of Bresolin et al. (2004) and our equations (4) and (11)–(12). Our abundance scale is close to that of Bresolin et al. (2004): the average difference between the original and rederived oxygen abundances for the H II regions of M51 is $\sim$0.03 dex. The open circles also show the data for two H II regions in the galaxy M101 (H1013 and H336) from Kennicutt et al. (2003) and for three H II regions in the galaxy NGC 1232 from Castellanos et al. (2002). The oxygen abundances of these additional H II regions have also been determined with the temperature-sensitive lines [S III] λ6312 and [N II] λ5755 and reduced to our abundance scale. For the object CDT1 in NGC 1232 (Castellanos et al. 2002), the O/H value rederived by Bresolin et al. (2004) has been adopted.

It is well known that the relation between the oxygen abundance and the strong oxygen line intensities is double valued, with two distinct parts traditionally known as the upper and lower branches of the R_{23}-O/H diagram. We have delimited in Figure 2 the upper and lower branches and the transition zone in between by horizontal lines, adopting $12 + \log(O/H) = 8.25$ as the boundary between the upper branch and the transition zone (*solid line*) and $12 + \log(O/H) = 8.00$ as the boundary between the transition zone and the lower branch (*dashed line*). These delimitations are somewhat arbitrary but were chosen so as to give the best calibrations with the existing data. Two distinct relations between the oxygen abundance and the strong oxygen line intensities are established, one for the upper branch (the high-metallicity calibration) and one for the lower branch (the low-metallicity calibration). But before discussing the calibrations, we need to find a way to eliminate low-quality measurements from our original sample. In the next section, we discuss

the selection criterion used to select out high-precision oxygen abundance measurements for high-metallicity H II regions.

3. THE DISCREPANCY INDEX

The sample defined in § 2.1 includes all H II regions we can find in the literature with a measured temperature-sensitive line ratio. The quality of the data is thus necessarily heterogeneous, with some measurements of the auroral [O III] λ4363 emission line having low accuracy. Moreover, Torres-Peimbert et al. (1989) have suggested that some early (prior to 1990) measurements of the [O III] λ4363 line fluxes obtained with nonlinear detectors give T_e-based oxygen abundances that are systematically overestimated, on average, by about 0.2 dex. Such problematic data can compromise the reliability of our strong oxygen line intensities–oxygen abundance calibration and need to be rejected. We thus require a criterion for selecting out only high-precision data.

Pilyugin (2000, 2001a, 2001b, 2003b) has advocated that the physical conditions in an H II region can be estimated via the excitation parameter P, i.e., by using only the strong oxygen nebular lines. If this is the case, then there must be a strong correlation between the oxygen auroral [O III] λ4363 and the nebular [O II] λ3727, [O III] $\lambda\lambda$4959, 5007 line fluxes in spectra of H II regions. Indeed, such a tight relationship has been found by Pilyugin (2005). The relation is found to be metallicity independent (or at least, if it does exist, any dependence is very weak) at high metallicities [$12 + \log(\mathrm{O/H}) \gtrsim 8.25$], in contrast to the situation at low metallicities for which it depends strongly on metallicity.

The top panel of Figure 3 shows the auroral line flux R (all fluxes are normalized to the Hβ flux) as a function of the total flux R_{23} in strong nebular lines for a sample of H II regions with oxygen line fluxes measured with high precision (see the definition of the sample and references in Pilyugin 2005). The oxygen abundances $12 + \log(\mathrm{O/H})$ of the H II regions vary between 8.25 and 8.6, and their excitation parameters P are in the range from $\sim$0.35 to $\sim$0.9. It is clear that all these high-metallicity H II regions with high-precision measurements lie along a single line, i.e., there is a one-to-one correspondence between the oxygen auroral and nebular line fluxes in the spectra of high-metallicity H II regions. This ff (flux-flux) relation can be described by the equation (Pilyugin 2005):

$$\log R = -4.264 + 3.087 \log R_{23}. \quad (14)$$

We can now make use of the ff relation to define a "discrepancy index" equal to the difference between the logarithm of the observed flux R in the [O III] λ4363 line and that of the flux R_{ff} of that line derived from the strong [O II] λ3727, [O III] $\lambda\lambda$4959, 5007 lines using the ff relation:

$$D_{\mathrm{ff}} = \log R_{\mathrm{ff}} - \log R. \quad (15)$$

This discrepancy index allows us to eliminate low-quality measurements with large D_{ff}, while retaining high-quality ones with small D_{ff}.

The ff relation can also be used to check the suggestion of Torres-Peimbert et al. (1989) that early T_e-based oxygen abundances are incorrect. We show in the middle panel of Figure 3 (*open circles*) the high-metallicity H II regions in our compilation with early (before 1990) measurements in the R-R_{23} diagram. It is clear that these H II regions show a systematic deviation from the ff relation of the top panel (*solid line*). The ff relation allows to estimate the auroral line flux R from the measured fluxes of the strong nebular lines and to determine the electron temperature in high-metallicity H II regions. Then the T_e method can be used to derive the oxygen abundance, which we designate by $(\mathrm{O/H})_{\mathrm{ff}}$. The difference between $(\mathrm{O/H})_{\mathrm{ff}}$ and $(\mathrm{O/H})_{T_e}$ for H II regions with early measurements is shown as a function of $(\mathrm{O/H})_{T_e}$ in the top panel of Figure 4. One can see that early $(\mathrm{O/H})_{T_e}$ determinations are systematically overestimated at metallicities higher than $12 + \log(\mathrm{O/H}) \gtrsim 8.4$. The bottom panel of Figure 4 shows the difference between $(\mathrm{O/H})_{\mathrm{ff}}$ and $(\mathrm{O/H})_{T_e}$ for H II regions with early measurements as a function of the discrepancy index D_{ff}. It can be seen that the condition $-0.1 < D_{\mathrm{ff}} < 0.1$, which we adopt, allows us to select out objects with differences between $\log(\mathrm{O/H})_{\mathrm{ff}}$ and $\log(\mathrm{O/H})_{T_e}$ less than $\simeq$0.1 dex.

We next check whether the measurements of low-excitation H II regions in the spiral galaxy M51 by Bresolin et al. (2004) are consistent with the ff relation. The spectra of these H II regions

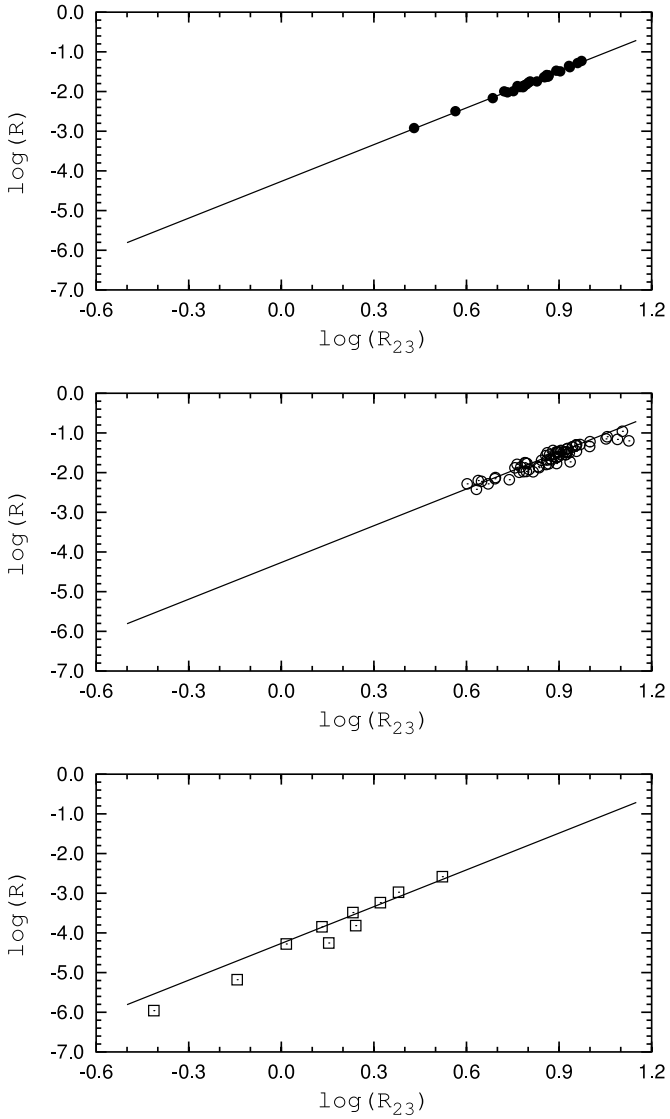

FIG. 3.—*Top*: Flux R in the auroral [O III] λ4363 line as a function of the total flux R_{23} in the strong nebular [O II] $\lambda\lambda$3727, 3729 and [O III] $\lambda\lambda$4959, 5007 lines for a sample of high-metallicity [$12 + \log(\mathrm{O/H}) > 8.25$] H II regions with high-precision measurements. The solid line (the ff relation) is the best fit to those data. *Middle*: R vs. R_{23} diagram for early (before 1990) measurements of high-metallicity H II regions from our compilation. The solid line is the same as in the top panel. *Bottom*: Estimated flux R in the auroral line as a function of the measured total flux R_{23} in the strong nebular lines for the low-excitation high-metallicity H II regions of Bresolin et al. (2004). The line is the same as in the top panel.

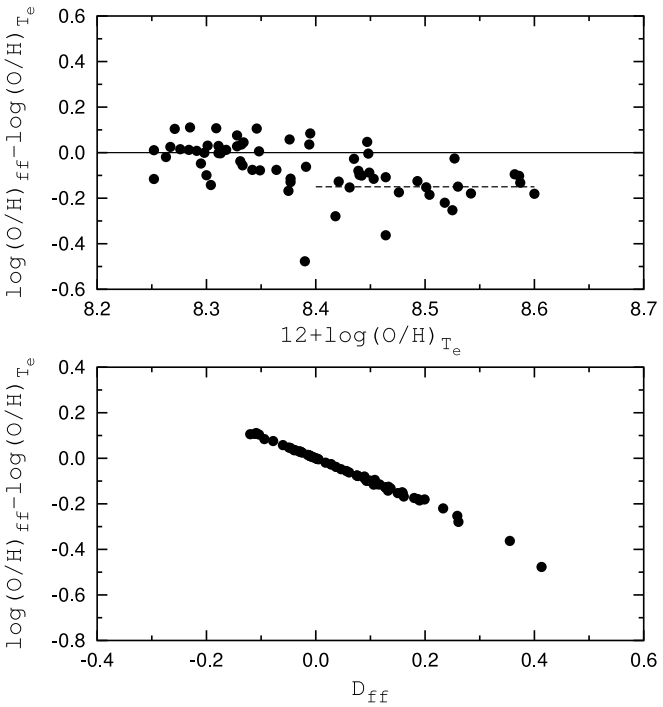

FIG. 4.—Differences between $(O/H)_{ff}$ and $(O/H)_{T_e}$ abundances for high-metallicity [$12 + \log(O/H) > 8.25$] H II regions with early (before 1990) measurements as a function of $(O/H)_{T_e}$ abundance (*top*) and as a function of the discrepancy index D_{ff} defined by eq. (15) (*bottom*).

show the auroral [S III] λ6312 line and/or the [N II] λ5755 line but not the auroral [O III] λ4363 line. The auroral line flux R flux was estimated from equation (7) using the electron temperature t_3 recommended by Bresolin et al. (2004). It is shown as a function of the total flux R_{23} in the bottom panel of Figure 3 (*open squares*) for the H II region sample of Bresolin et al. (2004). The solid line is the ff relation from the top panel. It is seen that the oxygen line fluxes in six faint high-metallicity H II regions (CCM 54, CCM 55, CCM 57, CCM 57A, CCM 71A, and CCM 84A) are in good agreement with the ff relation, while the remaining four (CCM 10, CCM 53, CCM 72, and P203) show significant deviations. The positions of those discrepant H II regions in the $t_{N\,II}$ versus $t_{S\,III}$ diagram of Bresolin et al. (2004, their Fig. 2) suggest that their electron temperature determinations should be accurate and, consequently, that their values of R estimated from the electron temperatures should be reliable. The deviation from the ff relation could be due to uncertainties in the nebular oxygen line fluxes and especially in the R_2 line flux, since it makes a dominant contribution to the R_{23} value, the flux in the R_3 line being small. If this is the case, then the measured R_2 fluxes in the four H II regions CCM 10, CCM 53, CCM 72, and P203 would be overestimated by 20%–30% [corresponding to an overestimate of $\sim$0.1 dex for the $(O/H)_{T_e}$ abundances], considerably larger than the errors of $\sim$10% in the measurements of Bresolin et al. (2004). We suggest that the deviations from the ff relation occur not because of flux measurement errors, but probably because the line fluxes measured within the slit do not reflect their relative contributions to the radiation of the nebula as a whole (Pilyugin 2005). This would happen, for example, if the relative fractions of the [O II] and [O III] zones in the slit differ significantly from those of the entire nebula. This effect would be more important for large H II regions, and it is interesting to note that at least three of the H II regions with large D_{ff} (CCM 10, CCM 72, and P203) have significantly larger angular diameters than the H II regions with small D_{ff} in the sample of Bresolin et al. (2004).

In the next two sections, we revisit the oxygen line intensities–O/H calibrations for both the upper and lower branches of the O/H-R_{23} diagram using $(O/H)_{T_e}$ abundances.

4. THE LINE INTENSITIES–O/H UPPER BRANCH CALIBRATION

The ff relation allows to estimate the auroral line flux R from the measured fluxes of the strong nebular lines and to determine electron temperatures in high-metallicity H II regions. Then the $(O/H)_{ff}$ abundance in H II regions can be obtained via the T_e method. In other words, the ff relation provides the possibility to estimate the oxygen abundance in high-metallicity H II regions using only strong nebular lines. However, we use the P method, rather than the ff relation, to calibrate because while the latter is independent of metallicities for $12 + \log O/H \geq 8.25$, it depends strongly on metallicity at lower metallicities. We use the ff relation only to derive D_{ff} and select out H II regions with high-quality measurements, those with an absolute value of $D_{ff} \leq 0.1$.

4.1. *Method*

To derive the relation between the oxygen abundance and the strong oxygen line intensities, we follow the approach of Pilyugin (2001a). The R_3-P diagram for our sample of high-metallicity H II regions with an absolute value of the discrepancy index D_{ff} less than 0.1 is shown in Figure 5. Those H II regions with $8.25 < 12 + \log(O/H) < 8.30$ are shown by filled circles, and those with $8.55 < 12 + \log(O/H) < 8.60$ by open circles. Inspection of Figure 5 suggests that the relation between R_3 and P can be fitted by a polynomial of the form

$$k_0 R_3 = k_1 P + k_2 P^2 + k_3 P^3. \quad (16)$$

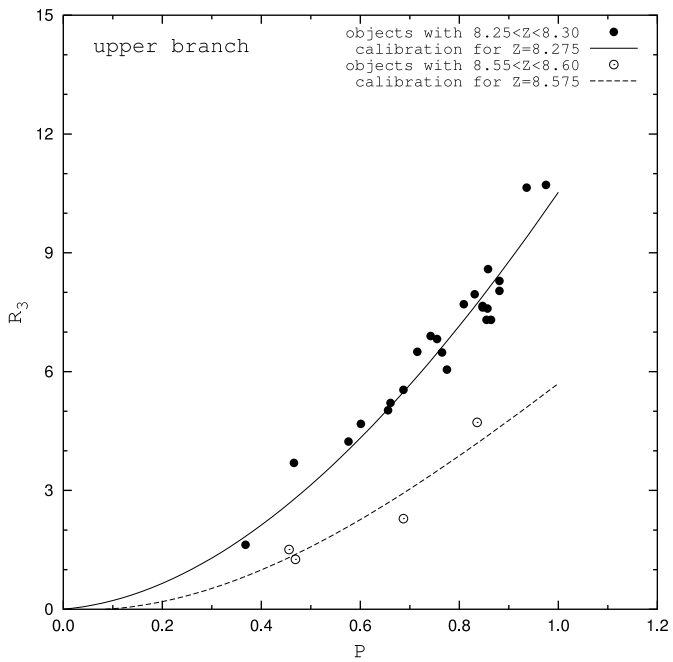

FIG. 5.—R_3-P diagram for high-metallicity H II regions. The filled circles are H II regions with $8.25 < 12 + \log(O/H) < 8.30$, and the open circles are those with $8.55 < 12 + \log(O/H) < 8.60$. The curves are computed with the derived calibration (eq. [21]) for two values of the oxygen abundance, $12 + \log(O/H) = 8.275$ (*solid line*) and $12 + \log(O/H) = 8.575$ (*dashed line*).

The zeroth-degree term of the polynomial must be equal to zero, since R_3 and P must be simultaneously null by definition. Figure 5 shows that the H II regions with $12 + \log(\mathrm{O/H}) = 8.25$–$8.30$ are shifted relative to those with $12 + \log(\mathrm{O/H}) = 8.55$–$8.60$, i.e., the position of a H II region in the R_3-P diagram depends on its metallicity. To take into account this metallicity dependence, the coefficients of equation (16) are chosen to have the form

$$k_j = a_j + b_j Z, \tag{17}$$

where we have used the notation $Z = 12 + \log(\mathrm{O/H})$ for brevity. Equation (16) can then be rewritten as

$$R_3 = \frac{(a_1 + b_1 Z)P + (a_2 + b_2 Z)P^2 + (a_3 + b_3 Z)P^3}{1 + b_0 Z}. \tag{18}$$

The coefficient a_0 is set to 1 (by dividing the numerator and the denominator on the right side of eq. [18] by a_0). Equation (18) can then be solved for Z:

$$Z = \frac{R_3 - a_1 P - a_2 P^2 - a_3 P^3}{b_1 P + b_2 P^2 + b_3 P^3 - b_0 R_3}. \tag{19}$$

Since $R_3 = PR_{23}$, equation (19) can be rewritten as

$$Z = \frac{R_{23} - a_1 - a_2 P - a_3 P^2}{b_1 + b_2 P + b_3 P^2 - b_0 R_{23}}. \tag{20}$$

The coefficients a_1, a_2, a_3, b_0, b_1, b_2, and b_3 can then be determined by looking for the best fit to our sample of H II regions with measured oxygen abundances. In other words, the position of an H II region in the R_3-P diagram can be calibrated in terms of its oxygen abundance.

4.2. *The Upper Branch Calibration*

The above set of coefficients can be derived by imposing two conditions. The first one is that the parameter $\langle \Delta(\mathrm{O/H}) \rangle = (\{\sum_{j=1}^{n} [\Delta(\mathrm{O/H})_j]^2\}/n)^{1/2}$ is minimum. Here $\Delta(\mathrm{O/H})_j$ is equal to $\log(\mathrm{O/H})_{P,j} - \log(\mathrm{O/H})_{T_e,j}$ for each H II region in our sample. The quantity $\langle \Delta(\mathrm{O/H}) \rangle$ is the average value of the differences between the oxygen abundances determined through the calibration and the original ones. The second condition requires that there is no systematic error in the (O/H)-values derived from the P method; i.e., $\Delta(\mathrm{O/H})$ does not show a dependence on either oxygen abundance or excitation parameter.

The obtained upper branch P calibration is

$$Z = \frac{R_3 + 726.1P + 842.2P^2 + 337.5P^3}{85.96P + 82.76P^2 + 43.98P^3 + 1.793R_3}, \tag{21}$$

or

$$Z = \frac{R_{23} + 726.1 + 842.2P + 337.5P^2}{85.96 + 82.76P + 43.98P^2 + 1.793R_{23}}. \tag{22}$$

Selecting only H II regions with $-0.1 < D_{\mathrm{ff}} < 0.1$, we used a total of 104 data points (out of 170 in the original sample) to derive the relation. We show $\Delta(\mathrm{O/H})$ for the individual H II regions as a function of oxygen abundance in Figure 6 (*top*) and as a function of the excitation parameter P (*bottom*). For the vast majority of the H II regions, the absolute value of $\Delta(\mathrm{O/H})$ does not exceed 0.1, irrespective of oxygen abundance or P. We also compare $(\mathrm{O/H})_P$ and $(\mathrm{O/H})_{\mathrm{ff}}$ abundances. The differences $(\mathrm{O/H})_P - (\mathrm{O/H})_{\mathrm{ff}}$ are shown by filled circles in Figure 7 as a function of $(\mathrm{O/H})_{\mathrm{ff}}$ abundance (*top*) and of P (*bottom*). Finally, we compare $(\mathrm{O/H})_P^*$ abundances, determined through the previous upper branch P calibration by Pilyugin (2001a), with $(\mathrm{O/H})_{\mathrm{ff}}$ abundances. The differences $(\mathrm{O/H})_P^* - (\mathrm{O/H})_{\mathrm{ff}}$ are shown in Figure 7 (*open circles*). Examination of Figure 7 reveals two facts. First, the differences between $(\mathrm{O/H})_{\mathrm{ff}}$ abundances and those derived through the P method are systematically larger for the old calibration as compared to the new calibration. The old P-based abundances are systematically greater than the $(\mathrm{O/H})_{\mathrm{ff}}$ abundances. On the other hand, there does not appear to be any strong systematic difference between $(\mathrm{O/H})_{\mathrm{ff}}$ abundances and the new P-based abundances for $12 + \log \mathrm{O/H} > 8.3$ and $P > 0.2$. In the top panel, the points with $12 + \log \mathrm{O/H} > 8.45$ lie systematically above the zero line, but by a very small amount ($\sim$0.01 dex). As for the points with $12 + \log \mathrm{O/H} < 8.3$, they lie systematically below the zero line, but the difference is also small, $\sim$0.03 dex. In the bottom panel, the lowest excitation point shows a large deviation above the zero line of $\sim$0.06 dex. Unfortunately, we have only one point with $P < 0.2$ in our sample and cannot say whether that deviation is meaningful. Overall, it is clear that the new P calibration is more accurate than the old one.

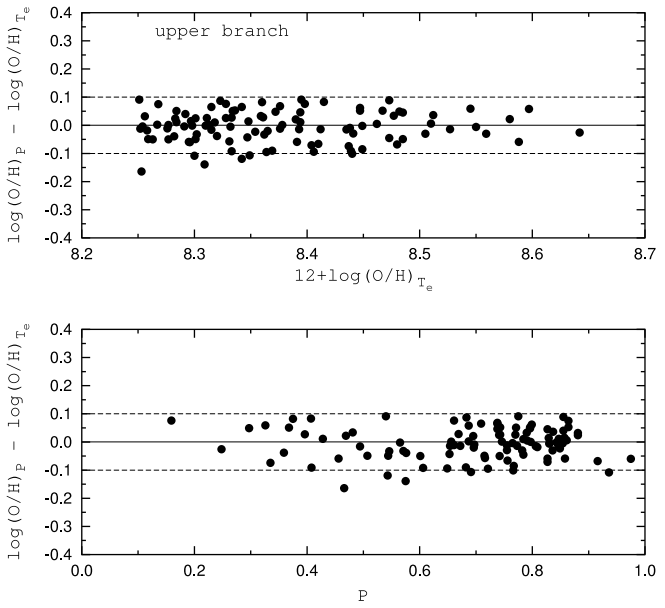

FIG. 6.—Differences between $(\mathrm{O/H})_P$ and $(\mathrm{O/H})_{T_e}$ abundances as a function of oxygen abundance (*top*) and of the excitation parameter P (*bottom*) for the high-metallicity H II regions with an absolute value of the discrepancy index D_{ff} less than 0.1.

The second feature of note is that the largest differences occur for low-excitation H II regions (Fig. 7, *bottom*). This is because in the old calibration, the calibrating sample of H II regions with T_e-based abundances was supplemented by a subsample of low-excitation H II regions with oxygen abundances estimated from the "oxygen abundance–galactocentric distance" relation, the R_G-based oxygen abundances, for which it was not possible to check the accuracy. In the new calibration, only T_e-based abundances are used, and the ff relation allows to select out high-precision measurements from them, making the new upper branch P calibration much more secure for low-excitation H II regions.

In summary, the $(\mathrm{O/H})_P$ abundances are close to $(\mathrm{O/H})_{\mathrm{ff}}$ abundances; i.e., they are as sensitive to the errors in the nebular

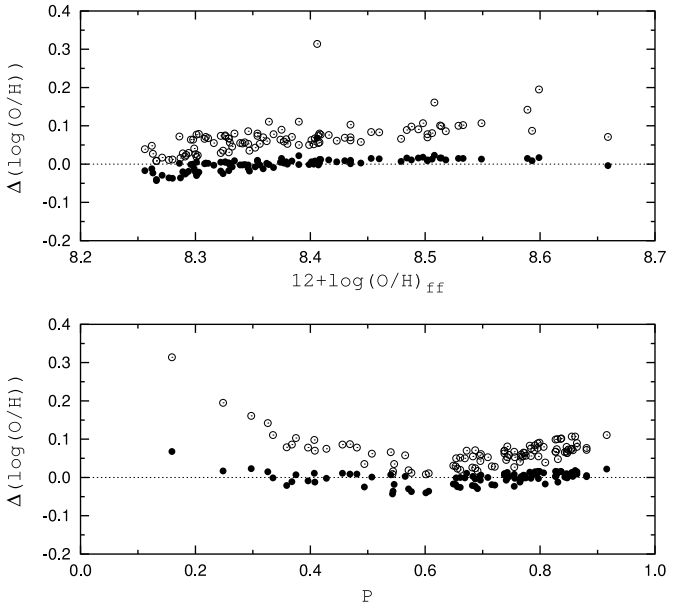

FIG. 7.—Differences between oxygen abundances $(O/H)_P$ derived with the new P calibration and $(O/H)_{ff}$ abundances (*filled circles*), and differences between oxygen abundances $(O/H)^*_P$ derived with the early P calibration from Pilyugin (2001a) and $(O/H)_{ff}$ abundances (*open circles*) as a function of $(O/H)_{ff}$ abundance (*top*) and of the excitation parameter P (*bottom*) for high-metallicity H II regions with an absolute value of the discrepancy index D_{ff} less than 0.1.

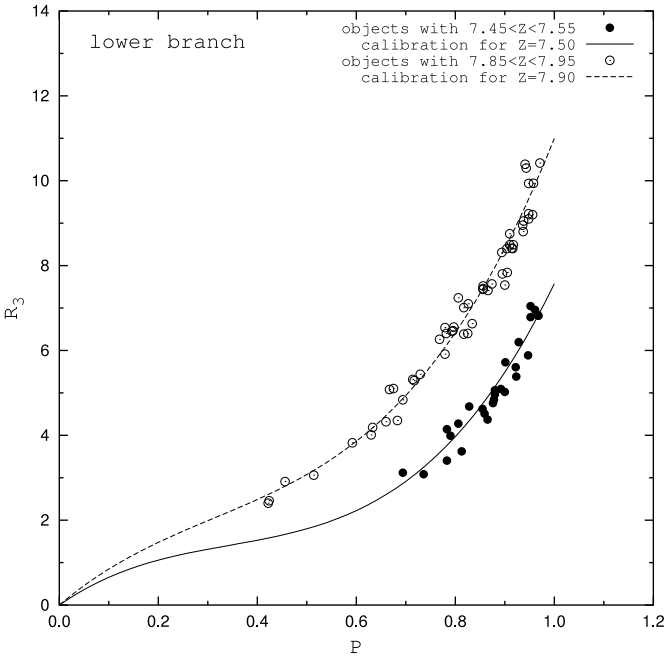

FIG. 8.—The R_3-P diagram for low-metallicity H II regions. The filled circles are H II regions with $7.45 < 12 + \log(O/H) < 7.55$ and the open circles are those with $7.85 < 12 + \log(O/H) < 7.95$. The lines are calculated from the derived calibration (eq. [23]) for $12 + \log(O/H) = 7.5$ (*solid line*) and for $12 + \log(O/H) = 7.9$ (*dashed line*).

line measurements as the $(O/H)_{ff}$ abundances. There are significant differences between oxygen abundances determined through the early and present P calibrations.

5. THE LINE INTENSITIES–O/H LOWER BRANCH CALIBRATION

5.1. *The Lower Branch Calibration*

We show the observed R_3-P diagram for low-metallicity H II regions in Figure 8. Those regions with $7.45 < 12 + \log(O/H) < 7.55$ are shown by filled circles, and those with $8.85 < 12 + \log(O/H) < 8.95$ by open circles. Like the high-metallicity H II regions in the upper branch, we see that the position of a low-metallicity H II region in the R_3-P diagram is dependent on its metallicity. Figure 8 shows that the positions of the H II regions with $12 + \log(O/H) = 7.45$–7.55 are shifted relative to those with $12 + \log(O/H) = 7.85$–7.95. Therefore, the same strategy applies for the search of a relation between the oxygen abundance and the strong oxygen line intensities for the lower branch of the R_{23}-O/H diagram.

We wish to derive a set of coefficients in equation (18) that gives the minimum value of $\langle\Delta(O/H)\rangle$ and results in no dependence of $\Delta(O/H)$ on abundance and excitation parameter, using our sample of low-metallicity H II regions. Unlike the case for high-metallicity objects, we do not have a criterion for selecting out low-metallicity H II regions with high-precision measurements. Instead, we use an iteration procedure in the construction of the lower branch P calibration. At each step, a relation is determined for the sample. Then data points with large deviations, in excess of $2\langle\Delta O/H\rangle$, are rejected, and a new relation is derived. The iteration converges after a number of steps ($\gtrsim 10$).

We have constructed the lower branch P calibration for two different samples. The first sample includes all low-metallicity H II regions as described in § 2.1. The final relation was obtained using 230 data points out of an original set of 318 points. The following values of the coefficients were obtained: $a_1 = -110.8$, $a_2 = -111.1$, $a_3 = 3.51$, $b_0 = 0.323$, $b_1 = 17.41$, $b_2 = 9.72$, and $b_3 = 5.36$. The second P calibration was constructed using only recent data, those obtained since 1995, so as to avoid problems with data obtained with nonlinear detectors. The final relation was obtained using 127 data points, out of an original set of 158 points. The final relation is of the form

$$Z = \frac{R_3 + 106.4P + 106.8P^2 - 3.40P^3}{17.72P + 6.60P^2 + 6.95P^3 - 0.302R_3}, \qquad (23)$$

or

$$Z = \frac{R_{23} + 106.4 + 106.8P - 3.40P^2}{17.72 + 6.60P + 6.95P^2 - 0.302R_{23}}. \qquad (24)$$

Figure 9 compares the $(O/H)_P$ abundances derived through the relation based on the total sample with those derived through the relation based on the sample with only data obtained since 1995. The solid line represents perfect agreement. It is clear that the two relations result in $(O/H)_P$ abundances that are very close to each other. We conclude that our lower branch P calibration is robust and that the iteration procedure has been effective in rejecting low-precision measurements in both samples. For definiteness's sake, we will adopt the P calibration based only on recent data, i.e., equations (23) and (24). In the following figures, only data with recent $(O/H)_{T_e}$ abundance determinations will be shown.

5.2. *Characteristics of the New Lower Branch Calibration*

The abundance differences $\Delta(O/H)$ between $(O/H)_P$ obtained with the present P calibration and those computed by the T_e method for low-metallicity H II regions are shown in Figure 10 as a function of the oxygen abundance (*top*) and as a function of the excitation parameter P (*bottom*). The points used in the

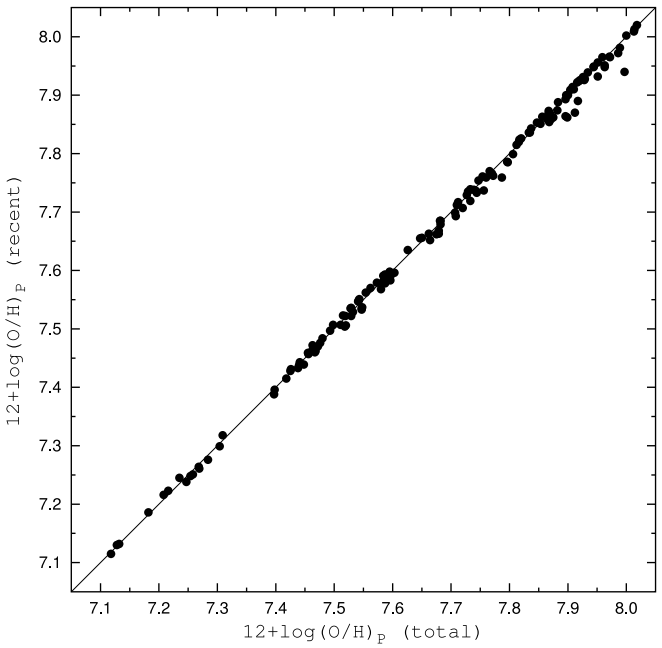

FIG. 9.—Oxygen abundances in low-metallicity H II regions determined through the *P* calibration based on only recent (since 1995) $(O/H)_{T_e}$ measurements versus oxygen abundances determined through the *P* calibration based on all measured $(O/H)_{T_e}$. The H II regions with recent line intensities measurements are shown by filled circles.

determination of the final relation, from the H II region sample with measurements since 1995, are shown by filled circles. Their dispersion about the zero line is ~0.1 dex in both panels, which is quite reasonable. For comparison, we also show by open circles the objects that have been rejected by the iteration procedure. It is evident that their deviation from the zero line is considerably larger. The $R_3 = f(P, Z)$ curves computed with

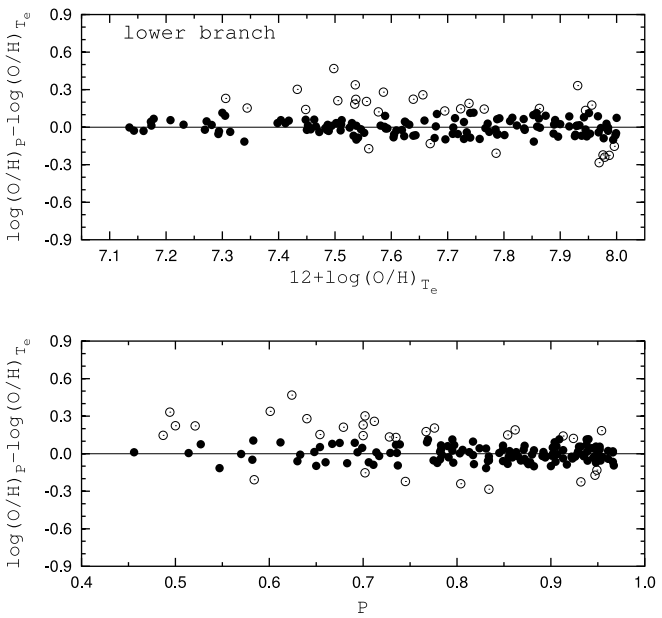

FIG. 10.—Differences between oxygen abundances $(O/H)_P$ derived from the present lower branch *P* calibration and T_e-based oxygen abundances $(O/H)_{T_e}$ as a function of oxygen abundance (*top*) and of the excitation parameter *P* (*bottom*) for the sample of H II regions with $(O/H)_{T_e}$ abundances measured since 1995. Filled circles show the H II regions used in the derivation of the final calibration (eqs. [23] and [24]). Open circles show the H II regions rejected by the iteration procedure.

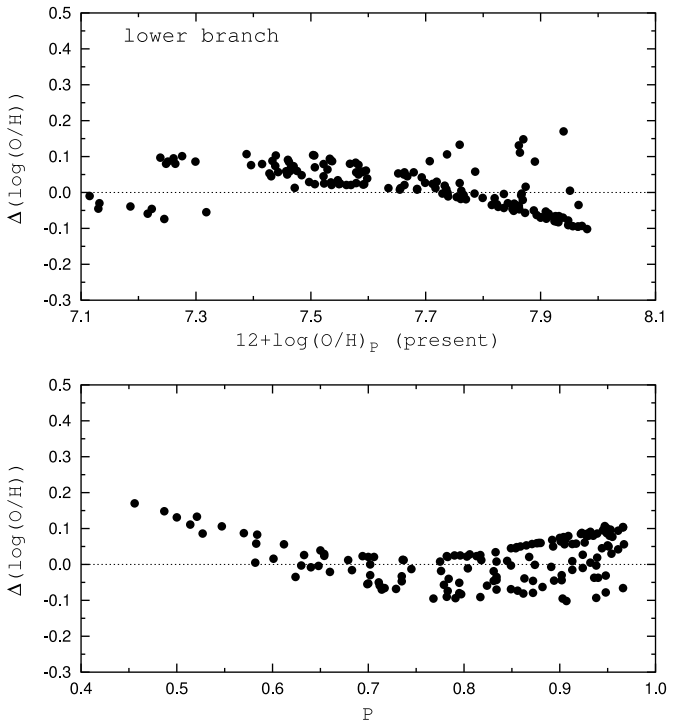

FIG. 11.—Differences between oxygen abundances derived with the early lower branch *P* calibration from Pilyugin (2001a) and with the present new *P* calibration as a function of oxygen abundance (*top*) and of the excitation parameter *P* (*bottom*) for the sample of low-metallicity H II regions with abundance measurements since 1995.

equation (23) for two fixed values of the oxygen abundance, $12 + \log(O/H) = 7.5$ and $12 + \log(O/H) = 7.9$, are shown in Figure 8 superimposed on the observational data. Here again, the agreement is satisfactory. There are only a few low-metallicity H II regions with $P < 0.55$ in our sample (Fig. 8 and Fig. 10, *bottom*). Therefore, our lower branch calibration provides reliable oxygen abundances only in low-metallicity H II regions with $P \gtrsim 0.55$.

We now compare the present lower branch calibration with the earlier one by Pilyugin (2000). The differences between oxygen abundances derived in the two calibrations are shown in Figure 11 as a function of oxygen abundance (*top*) and of *P* (*bottom*). The distribution of the differences with metallicity in the top panel shows an evident curvature. This curvature is caused by the earlier assumption by Pilyugin (2000) that low-metallicity H II regions with the same *P* lie along a straight line in the O/H-R_{23} diagram. That assumption has been relaxed in the present calibration. The abundance differences also show a curved distribution as a function of the excitation parameter (Fig. 11, *bottom*). This systematic effect is probably due to the fact that the early low-metallicity calibration was based mainly on high-excitation H II regions. There were only a few calibrating H II regions with $P \lesssim 0.8$, which makes the relation unreliable in that domain. The present low-metallicity calibration should be reliable for H II regions with *P* in the range from ~0.55 to ~1.

6. THE VALIDITY OF THE *P* CALIBRATION

6.1. *Preliminary Remarks*

The validity and reliability of the early upper branch *P* calibration has been questioned by Bresolin et al. (2004). They have compared O/H abundances derived through the early

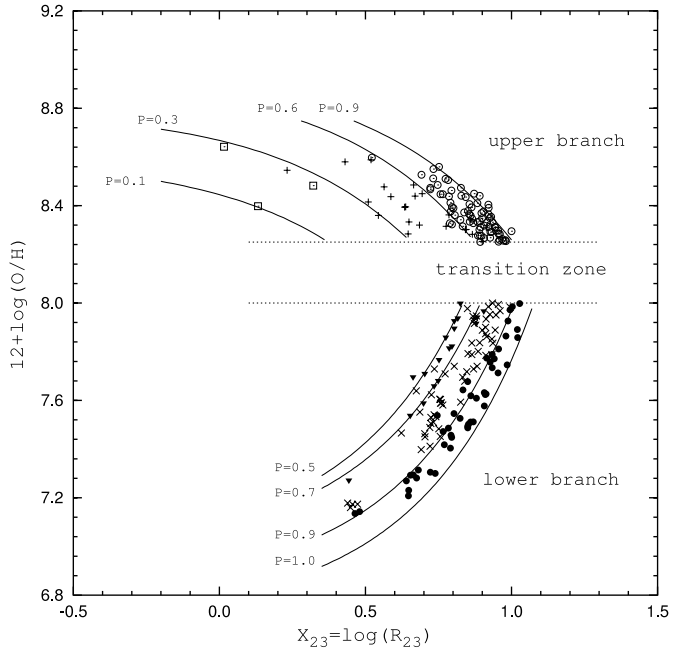

FIG. 12.—Family of $O/H = f(R_{23}, P)$ curves labeled by different values of the excitation parameter P, superimposed on the observational data. The high-metallicity H II regions with $0.0 < P < 0.3$ are shown by open squares, those with $0.3 < P < 0.6$ by plus signs, and those with $0.6 < P < 0.9$ by open circles. The low-metallicity H II regions with $0.5 < P < 0.7$ are shown by filled triangles, those with $0.7 < P < 0.9$ by crosses, and those with $0.9 < P < 1.0$ by filled circles.

upper branch P calibration with their own and published measured abundances (their Fig. 9) and have concluded that the P calibration suffers from severe difficulties in a wide abundance range.

These questions of validity and reliability can be addressed on two levels, first on the general level and second, on a more particular level. On the general level, one may question the assumption on which the P calibration relies, that the strong oxygen lines [O II] $\lambda\lambda$3727, 3729 and [O III] $\lambda\lambda$4959, 5007 contain the necessary information for determining accurate oxygen abundances in H II regions. The uncovering of the tight empirical ff relation (Pilyugin 2005 and Fig. 3, *top*) confirms that this assumption is correct.

On a more detailed level, the particular form of the analytical expression adopted for the upper branch P calibration may be questioned. We have chosen a simple form, but perhaps a more complex expression may give a better fit to the oxygen abundance–strong line fluxes relationship. Furthermore, the coefficients in the adopted expression are derived using calibrating H II regions that have a discrepancy index $D_{\rm ff}$ as large as 0.1 dex in absolute value. Perhaps smaller absolute values of $D_{\rm ff}$ may result in a more precise relation. To check these issues, we have plotted the R_{23}-O/H diagram for H II regions with $-0.1 < D_{\rm ff} < 0.1$ in Figure 12. Superimposed on the observational data are shown $O/H = f(R_{23}, P)$ curves calculated for different values of P. High-metallicity H II regions with $0.0 < P < 0.3$ are shown by open squares, those with $0.3 < P < 0.6$ by plus signs, and those with $0.6 < P < 0.9$ by open circles. Low-metallicity H II regions with $0.5 < P < 0.7$ are shown by filled triangles, those with $0.7 < P < 0.9$ by crosses, and those with $0.9 < P < 1.0$ by filled circles. It can be seen that the calibration curves give a satisfactory fit to the observational data. At the same time, Figure 12 shows that the available high-precision measurements for calibrating low-excitation H II regions (with $P \lesssim 0.4$) are very few in number.

6.2. *The* $(O/H)_P$ *versus* $(O/H)_{T_e}$ *Diagram*

We next check the integrity of our calibration by comparing the $(O/H)_P$ abundances determined through the present upper branch P calibration and the $(O/H)_{\rm ff}$ abundances with the $(O/H)_{T_e}$ abundances determined by Bresolin et al. (2004) for a sample of H II regions in the spiral galaxy M51. Figure 13 shows the $(O/H)_P$ versus $(O/H)_{T_e}$ diagram (the analog of Fig. 9 of Bresolin et al. 2004) for our calibrating sample of high-metallicity H II regions with $-0.1 < D_{\rm ff} < 0.1$ (*open circles*). The H II region sample of Bresolin et al. (2004) is shown by filled circles. As discussed in Figure 6 , the vast majority of the points in our sample fall within ± 0.1 dex (*dashed lines*) of the perfect agreement (*solid line*). Six out of the 10 objects in the Bresolin et al. (2004) sample do the same. The remaining four show a large discrepancy. As discussed in § 3, it appears that their oxygen abundances are overestimated.

Comparison of Figure 13 with Figure 9 of Bresolin et al. (2004) shows a considerably larger scatter in the latter, for both high $(12 + \log O/H > 8.25)$ and low $(12 + \log O/H < 8.25)$ metallicities. There are two reasons for the larger differences between $(O/H)_{T_e}$ and $(O/H)_P$ at high metallicities in the diagram of Bresolin et al. (2004). First, the upper branch P calibration in the present work is based on T_e-based abundances only, while both T_e-based and the "surrogate" R_G-based abundances were used in the construction of the previous P calibration. The new upper branch P calibration results in considerably smaller differences between $(O/H)_{T_e}$ and $(O/H)_P$ at low excitation. Second, Bresolin et al. (2004) used in their comparison the original T_e-based abundances from different authors. These can be inconsistent with each other, thus producing a larger dispersion. For example, Bresolin et al. (2004) derived, by using Castellanos et al.'s (2002) line fluxes for the H II region CDT1 in NGC 1232, a log O/H value smaller by 0.13 dex than the abundance published

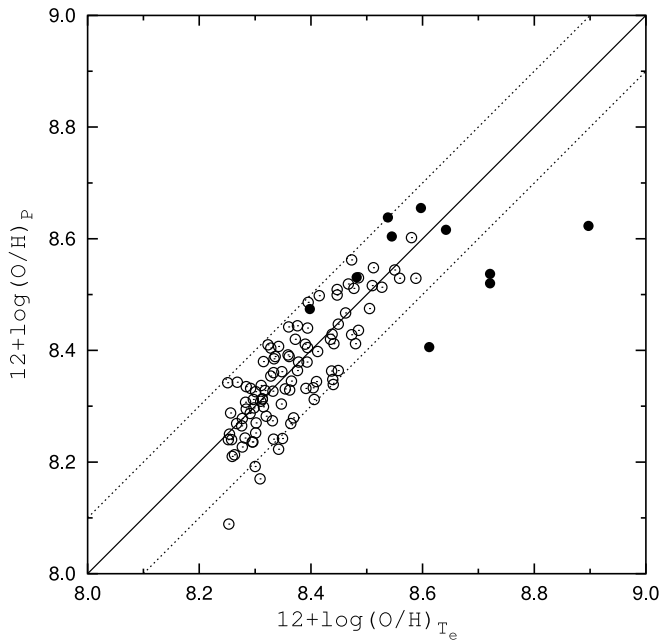

FIG. 13.—$(O/H)_P$ abundances vs. $(O/H)_{T_e}$ abundances for the sample of high-metallicity H II regions with $-0.1 < D_{\rm ff} < 0.1$ (*open circles*). The H II regions of the spiral galaxy M51 from Bresolin et al. (2004) are shown by filled circles.

by those authors. On the other hand, to carry out our comparison, we have used a homogeneous data set of T_e-based abundances of H II regions rescaled to the same T_e-based abundance system used in the construction of the calibration. Thus, we conclude that with the present calibration, there is satisfactory agreement between $(O/H)_{T_e}$ and $(O/H)_P$ abundances for high-metallicity H II regions with accurate line fluxes measurements.

We next discuss the comparison between $(O/H)_{T_e}$ and $(O/H)_P$ abundances at the low-metallicity end of the diagram in Figure 9 of Bresolin et al. (2004). These authors found a considerably larger disagreement for low-metallicity objects. We attribute this large disagreement to a misapplication of the P calibration. Any empirical relationship between the oxygen abundance and strong oxygen line intensities (including the P calibration) is double valued with two distinct parts, usually called the "lower" and "upper" branches of the R_{23}-O/H relationship. To use the calibration, one has to know a priori on which of the two branches the H II region lies. The upper branch P calibration is valid only for those H II regions that belong to the upper branch. Bresolin et al. (2004) noted that they plotted only objects that the P method predicts to have $12 + \log(O/H)_P > 8.2$, the quoted range of validity for this method in the high-abundance regime. But they derive $12 + \log(O/H)_P$ by assuming that the H II region lies on the upper branch, which is not necessarily the case. In fact, Figure 9 of Bresolin et al. (2004) also includes low-metallicity H II regions, with $12+ \log(O/H)_{T_e}$ lower than $\sim$8.2, which do not belong to the upper branch. In those cases, applying to them the upper branch P calibration would result in an overestimate of the oxygen abundance in low-metallicity H II regions to values of $12 + \log(O/H) \gtrsim 8.2$ (Pilyugin 2003a). This would account for the large differences between $(O/H)_{T_e}$ and $(O/H)_P$ abundances at low metallicities in Figure 9 of Bresolin et al. (2004). The problem of the misapplication of the upper branch of the P calibration is discussed more in detail by Pilyugin et al. (2004) in their study of the radial abundance distribution in the disks of spiral galaxies.

6.3. *The Radial Oxygen Abundance Distribution in the Spiral Galaxy M51*

Comparison between the radial oxygen abundance distributions as traced by $(O/H)_{T_e}$, $(O/H)_{ff}$, and $(O/H)_P$ abundances in the disk of the spiral galaxy M51 can also provide a check on the reliability of $(O/H)_P$ abundances.

The filled circles in Figure 14 show $(O/H)_{T_e}$ abundances (recomputed here so as to be on our abundance scale) for the H II regions of Bresolin et al. (2004). The dashed line is those authors' linear regression to these abundances:

$$12 + \log(O/H)_{T_e} = 8.72(\pm0.09) - 0.28(\pm0.14)R_G/R_{25}. \quad (25)$$

The open squares represent $(O/H)_{ff}$ abundances for the 11 H II regions in Bresolin et al.'s (2004) sample with small angular diameters. The nebular line measurements were taken from their Table 1 for the H II regions CCM 54, CCM 55, CCM 57, CCM 57A, CCM 71A, and CCM 84A and from their Table 6 for the H II regions CCM 6A, CCM 37A, CCM 45, CCM 56, and CCM 107. The solid line is the least-squares fit to the $(O/H)_{ff}$ abundances:

$$12 + \log(O/H)_{ff} = 8.74(\pm0.08) - 0.27(\pm0.15)R_G/R_{25}. \quad (26)$$

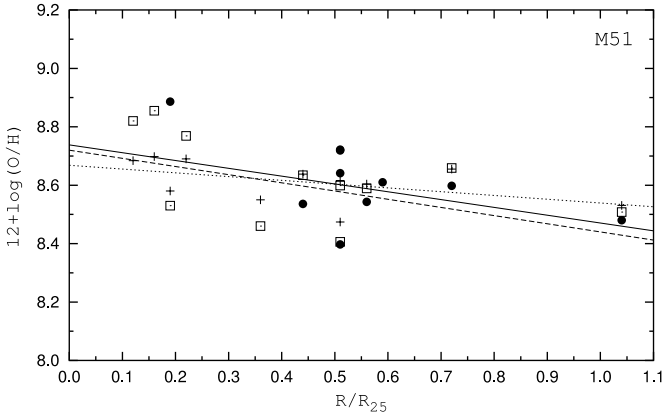

FIG. 14.—Radial distribution of oxygen abundance in the disk of the spiral galaxy M51. Filled circles are $(O/H)_{T_e}$ abundances for H II regions from Bresolin et al. (2004), open squares are $(O/H)_{ff}$ abundances for 11 H II regions, and plus signs are $(O/H)_P$ abundances for the same 11 H II regions. The solid line is the least-squares fit to $(O/H)_{ff}$ abundances and the dotted line is the least-squares fit to $(O/H)_P$ abundances. The dashed line is the original least-squares fit of Bresolin et al. (2004) to $(O/H)_{T_e}$ abundances.

The plus signs denote $(O/H)_P$ abundances for the same 11 H II regions. The dotted line is the least-squares fit to these $(O/H)_P$ abundances:

$$12 + \log(O/H)_P = 8.67(\pm0.04) - 0.13(\pm0.08)R_G/R_{25}. \quad (27)$$

Figure 14 shows that the gradients traced by the $(O/H)_{ff}$ and $(O/H)_{T_e}$ abundances are very similar (compare eq. [26] with eq. [25]). However the gradient traced by the $(O/H)_P$ abundances is shallower that the $(O/H)_{T_e}$ gradient obtained by Bresolin et al. (2004) (compare eq. [27] with eq. [25]), although they are consistent with each other within the uncertainties. The central oxygen abundances of the three fits agree to within 0.1 dex.

Taking into account the uncertainties, we conclude that there is an overall satisfactory agreement between the radial gradients traced by the $(O/H)_{T_e}$, $(O/H)_{ff}$, and $(O/H)_P$ abundances in the disk of M51.

7. CONCLUSIONS

We have revisited the problem of oxygen abundance determination in H II regions using the "strong oxygen line intensities–oxygen abundance" calibration. To this end, we have compiled a list of more than 700 spectroscopic measurements of H II regions in spiral and irregular galaxies with a measured intensity of the [O III] λ4363 line. We have recomputed in a homogeneous way their oxygen abundances through the T_e method and devised ways to select out high-precision measurements from the sample. We have used the high-precision sample to recalibrate the relation $O/H = f(R_{23}, P)$ between the oxygen abundance, the abundance index R_{23} introduced by Pagel et al. (1979), and the excitation parameter P of Pilyugin (2000). The calibration has been carried out empirically both at low metallicities for the lower branch of the O/H-R_{23} diagram and at high metallicities for the upper branch.

We also discuss an alternative way of deriving the oxygen abundance $(O/H)_{ff}$ in high-metallicity H II regions from the strong oxygen nebular lines only, using the ff relation (Pilyugin 2005) to estimate the flux in the auroral [O III] λ4363 line from

the measured fluxes in the nebular [O II] $\lambda\lambda$3727, 3729 and [O III] $\lambda\lambda$4959, 5007 lines.

The present calibration represents a significant improvement over the earlier one by Pilyugin (2000, 2001a) for several reasons, as follows:

1. The calibrating sample is considerably larger at both low and high metallicities. Ways have been devised to reject low-precision measurements.

2. The newly derived low-metallicity lower branch calibration is robust: the relations derived with the total $(O/H)_{T_e}$ sample and with the one containing only recent (obtained within the last 10 years) observations are in good agreement with each other. The differences in the derived $(O/H)_P$ abundances using these two relations are usually less than 0.02 dex. Both relations have been derived using an iteration procedure that retains only high-precision measurements.

3. The simplified assumption that H II regions with the same P lie along the same straight line in the O/H-R_{23} diagram by Pilyugin (2000) in his early lower branch calibration is relaxed in the present calibration. For the new lower branch calibration, the range of the excitation parameter P has been extended from $\sim$0.8–$\sim$1 to $\sim$0.55–$\sim$1.

4. The new high-metallicity upper branch calibration is determined on the basis of $(O/H)_{T_e}$ abundances only, while both T_e-based and "surrogate" R_G-based abundances were used in the construction of the previous upper branch P calibration. Moreover, only high-precision measurements selected via the ff relation have been used to derive the upper branch P calibration.

5. The $(O/H)_P$ abundances are usually close to the $(O/H)_{ff}$ abundances, although systematic differences as large as $\sim$0.1 dex between $(O/H)_{ff}$ and $(O/H)_P$ abundances can occur in faint ($\log R_{23} \lesssim -0.5$), low-excitation ($P \lesssim 0.25$) H II regions.

6. The T_e-derived oxygen abundances, on which the low- and high-metallicity calibrations are based, are determined consistently on the same abundance scale, which was not the case before. At both low and high metallicities, the new calibration gives $(O/H)_P$ abundances that agree with $(O/H)_{T_e}$ abundances to within 0.1 dex.

We thank Yuri Izotov and Grazyna Stasińska for providing us with a new set of T_e equations in advance of publication. We also thank them and Natalia Guseva for useful discussions. Bernard Pagel provided useful comments on a preliminary version of this paper. We thank the anonymous referee for helpful comments. L. S. P. is grateful for the hospitality of the Astronomy Department of the University of Virginia, where part of this investigation was carried out. The research described in this publication was made possible in part by award UP1-2551-KV-03 of the U.S. Civilian Research and Development Foundation for the Independent States of the Former Soviet Union (CRDF). L. S. P. was also partly supported by grant 02.07/00132 from the Ukrainian Fund of Fundamental Investigations. T. X. T. is grateful for the partial financial support of NSF grant AST 02-05785.

REFERENCES

Alloin, D., Collin-Souffrin, S., Joly, M., & Vigroux, L. 1979, A&A, 78, 200
Augarde, R., Figon, P., Vanderriest, C., & Lemonnier, J. P. 1990, A&A, 233, 348
Axon, D. J., Staveley-Smith, L., Fosbury, R. A. E., Danziger, J., Boksenberg, A., & Davies, R. D. 1988, MNRAS, 231, 1077
Baldwin, J. A., Verner, E. M., Verner, D. A., Ferland, G. J., Martin, P. G., Korista, K. T., & Rubin, R. H. 2000, ApJS, 129, 229
Bergvall, N. 1985, A&A, 146, 269
Bergvall, N., & Östlin, G. 2002, A&A, 390, 891
Bresolin, F., Garnett, D. R., & Kennicutt, R. C., Jr. 2004, ApJ, 615, 228
Campbell, A., Terlevich, R., & Melnick, J. 1986, MNRAS, 223, 811
Caplan, J., Deharveng, L., Peña, M., Costero, R., & Blondel, C. 2000, MNRAS, 311, 317
Castellanos, M., Díaz, A. I., & Terlevich, E. 2002, MNRAS, 329, 315
de Blok, W. J. G., & van der Hulst, J. M. 1998, A&A, 335, 421
de Naray, R. K., McGaugh, S. S., & de Blok W. J. G. 2004, MNRAS, 355, 887
Díaz, A. I., Terlevich, E., Pagel, B. E. J., Vílchez, J. M., & Edmunds, M. G. 1987, MNRAS, 226, 19
Dinerstein, H. L., & Shields, G. A. 1986, ApJ, 311, 45
Dopita M. A., & Evans I. N. 1986, ApJ, 307, 431
Dufour, R. J. 1975, ApJ, 195, 315
Dufour, R. J., & Harlow, W. V. 1977, ApJ, 216, 706
Durret, F., Bergeron, J., & Boksenberg, A. 1985, A&A, 143, 347
Edmunds, M. G., & Pagel, B. E. J. 1984, MNRAS, 211, 507
Esteban, C., Peimbert, M., García-Rojas, J., Ruiz, M. T., Peimbert, A., & Rodríguez, M. 2004, MNRAS, 355, 229
Esteban, C., Peimbert, M., Torres-Peimbert, S., & Escalante, V. 1998, MNRAS, 295, 401
Esteban, C., Peimbert, M., Torres-Peimbert, S., & García-Rojas, J. 1999a, Rev. Mex. AA, 35, 65
Esteban, C., Peimbert, M., Torres-Peimbert, S., García-Rojas, J., & Rodríguez, M. 1999b, ApJS, 120, 113
Fierro, J., Torres-Peimbert, S., & Peimbert, M. 1986, PASP, 98, 1032
French, H. B. 1980, ApJ, 240, 41
Fricke, K. J., Izotov, Y. I., Papaderos, P., Guseva, N. G., & Thuan, T. X. 2001, AJ, 121, 169
García-Rojas, J., Esteban, C., Peimbert, M., Rodríguez, M., Ruiz, M. T., & Peimbert, A. 2004, ApJS, 153, 501
Garnett, D. R. 1992, AJ, 103, 1330
Garnett, D. R., & Kennicutt, R. C., Jr. 1994, ApJ, 426, 123
Garnett, D. R., Shields, G. A., Peimbert, M., Torres-Peimbert, S., Skillman, E. D., Dufour, R. J., Terlevich, E., & Terlevich, R. J. 1999, ApJ, 513, 168
Garnett, D. R., Shields, G. A., Skillman, E. D., Sagan, S. P., & Dufour, R. J. 1997, ApJ, 489, 63
Gonzalez-Delgado, R., et al. 1994, ApJ, 437, 239
Gonzalez-Riestra, R., Rego, M., & Zamorano, J. 1987, A&A, 186, 64
———. 1988, A&A, 202, 27
Guseva, N. G., Izotov, Y. I., & Thuan, T. X. 2000, ApJ, 531, 776
Guseva, N. G., Papaderos, P., Izotov, Y. I., Green, R. F., Fricke, K. J., Thuan, T. X., & Noeske, K. G. 2003a, A&A, 407, 75
———. 2003b, A&A, 407, 91
———. 2003c, A&A, 407, 105
Guseva, N. G., Papaderos, P., Izotov, Y. I., Noeske, K. G., & Fricke, K. J. 2004, A&A, 421, 519
Guseva, N. G., et al. 2001, A&A, 378, 756
Heydari-Malayeri, M., Melnick, J., & Martin, J.-M. 1990, A&A, 234, 99
Hidalgo-Gámez, A. M., Masegosa, J., & Olofsson, K. 2001a, A&A, 369, 797
Hidalgo-Gámez, A. M., Olofsson, K., & Masegosa, J. 2001b, A&A, 367, 388
Hodge, P., & Miller, B. W. 1995, ApJ, 451, 176
Izotov Y. I., Chaffee, F. H., Foltz, C. B., Green, R. F., Guseva, N. G., & Thuan, T. X. 1999, ApJ, 527, 757
Izotov, Y. I., Chaffee, F. H., & Green, R. F. 2001a, ApJ, 562, 727
Izotov, Y. I., Chaffee, F. H., & Schaerer, D. 2001b, A&A, 378, L45
Izotov, Y. I., Dyak, A. B., Chaffee, F. H., Foltz, C. B., Kniazev, A. Y., & Lipovetsky, V. A. 1996, ApJ, 458, 524
Izotov, Y. I., Guseva, N. G., Lipovetsky, V. A., Kniazev, A. Y., & Stepanian, J. A. 1991, A&A, 247, 303
Izotov, Y. I., Papaderos, P., Guseva, N. G., Fricke, K. J., & Thuan, T. X. 2004, A&A, 421, 539
Izotov, Y. I., Stasinska, G., Meynet, G., Guseva, N. G., & Thuan, T. X. 2005, A&A, submitted
Izotov, Y. I., & Thuan, T. X. 1998a, ApJ, 497, 227
———. 1998b, ApJ, 500, 188
———. 2004, ApJ, 602, 200
Izotov, Y. I., Thuan, T. X., & Lipovetsky, V. A. 1994, ApJ, 435, 647
———. 1997, ApJS, 108, 1
Kennicutt, R. C., Jr., Bresolin, F., & Garnett, D. R. 2003, ApJ, 591, 801
Kennicutt, R. C., Jr., & Skillman, E. D. 2001, AJ, 121, 1461

Kewley L. J., & Dopita M. A. 2002, ApJS, 142, 35
Kinman, T. D., & Davidson, K. 1981, ApJ, 243, 127
Kniazev, A. Y., Grebel, E. K., Hao, L., Strauss, M. A., Brinkmann, J., & Fukugita, M. 2003, ApJ, 593, L73
Kobulnicky, H. A., Kennicutt, R. C., Jr., & Pizagno, J. L. 1999, ApJ, 514, 544
Kobulnicky, H. A., & Skillman, E. D. 1996, ApJ, 471, 211
———. 1997, ApJ, 489, 636
———. 1998, ApJ, 497, 601
Kobulnicky, H. A., Skillman, E. D., Roy, J.-R., Walsh, J. R., & Rosa, R. 1997, ApJ, 477, 679
Kunth, D., & Joubert, M. 1985, A&A, 142, 411
Kunth, D., & Sargent, W. L. W. 1983, ApJ, 273, 81
Kurt, C. M., Dufour, R. J., Garnett, D. R., Skillman, E. D., Mathis, J. S., Peimbert, M., Torres-Peimbert, S., & Ruiz, M.-T. 1999, ApJ, 518, 246
Kwitter, K. B., & Aller, L. H. 1981, MNRAS, 195, 939
Lee, H., McCall, M. L., Kingsburgh, R. L., Ross, R., & Stevenson, C. C. 2003a, AJ, 125, 146
Lee, H., McCall, M. L., & Richer, M. G. 2003b, AJ, 125, 2975
Lee, H., Skillman, E. D., & Venn, K. A. 2005, ApJ, 620, 223
Lequeux, J., Peimbert, M., Rayo, J. F., Serrano, A., & Torres-Peimbert, S. 1979, A&A, 80, 155
Luridiana, V., Esteban, C., Peimbert, M., & Peimbert, A. 2002, Rev. Mex. AA, 38, 97
McCall, M. L., Rybski, P. M., & Shields, G. A. 1985, ApJS, 57, 1
McGaugh, S. S. 1991, ApJ, 380, 140
———. 1994, ApJ, 426, 135
Melbourne, J., Phillips, A., Salzer, J. J., Gronwall, C., & Sarajedini, V. 2004, AJ, 127, 686
Melnick, J., Heydari-Malayeri, M., & Leisy, P. 1992, A&A, 253, 16
Miller, B. W. 1996, AJ, 112, 991
Miller, B. W., & Hodge, P. 1996, ApJ, 458, 467
Moles, M., Aparicio, A., & Masegosa, J. 1990, A&A, 228, 310
Noeske, K. G., Guseva, N. G., Fricke, K. J., Izotov, Y. I., Papaderos, P., & Thuan, T. X. 2000, A&A, 361, 33
O'Connell, R. W., Thuan, T. X., & Goldstein, S. J. 1978, ApJ, 226, L11
Oey, M. S., & Shields, J. C. 2000, ApJ, 539, 687
Osterbrock, D. E., Tran, H. D., & Veilleux, S. 1992, ApJ, 389, 305
Pagel, B. E. J., Edmunds, M. G., Blackwell, D. E., Chun, M. S., & Smith, G. 1979, MNRAS, 189, 95
Pagel, B. E. J., Edmunds, M. G., & Smith, G. 1980, MNRAS, 193, 219
Pagel, B. E. J., Simonson, E. A., Terlevich, R. J., & Edmunds, M. G. 1992, MNRAS, 255, 325
Peimbert, A. 2003, ApJ, 584, 735
Peimbert, M. 1967, ApJ, 150, 825
Peimbert, M., Peimbert, A., & Ruiz, M. T. 2000, ApJ, 541, 688
Peimbert, M., & Torres-Peimbert, S. 1974, ApJ, 193, 327
———. 1976, ApJ, 203, 581
———. 1992, Rev. Mex. AA, 24, 155
Peimbert, M., Torres-Peimbert, S., & Dufour, R. J. 1993, ApJ, 418, 760
Pilyugin, L. S. 2000, A&A, 362, 325
———. 2001a, A&A, 369, 594
———. 2001b, A&A, 373, 56
———. 2003a, A&A, 397, 109
Pilyugin, L. S. 2003b, A&A, 399, 1003
———. 2005, A&A, 436, 1L
Pilyugin, L. S., Vílchez, J. M., & Contini, T. 2004, A&A, 425, 849
Popescu, C. C., & Hopp, U. 2000, A&AS, 142, 247
Pustilnik, S. A., Kniazev, A. Y., Masegosa, J., Márquez, I., Pramskij, A. G., & Ugryumov, A. V. 2002, A&A, 389, 779
Pustilnik, S. A., Kniazev, A., Pramskij, A., Izotov, I., Foltz, C., Brosh, N., Martin, J.-M., & Ugryumov, A. 2004, A&A, 419, 469
Pustilnik, S. A., Kniazev, A. Y., Pramskij, A. G., Ugryumov, A. V., & Masegosa, J. 2003a, A&A, 409, 917
Pustilnik, S., Zasov, A., Kniazev, A., Pramskij, A., Ugryumov, A., & Burenkov, A. 2003b, A&A, 400, 841
Rayo, J. F., Peimbert, M., & Torres-Peimbert, S. 1982, ApJ, 255, 1
Rego, M., Cordero-Gracia, M., Gallego, J., & Zamorano, J. 1998, A&A, 330, 435
Rönnback, J., & Bergvall, N. 1995, A&A, 302, 353
Rosa, M., & Mathis, J. S. 1987, ApJ, 317, 163
Shaver, P. A., McGee, R. X., Newton, L. M., Danks, A. C., & Pottash, S. R. 1983, MNRAS, 204, 53
Shields, G. A., & Searle, L. 1978, ApJ, 222, 821
Skillman, E. D. 1985, ApJ, 290, 449
Skillman, E. D., Côté, S., & Miller, B. W. 2003, AJ, 125, 610
Skillman, E. D., & Kennicutt, R. C. 1993, ApJ, 411, 655
Skillman, E. D., Kennicutt, R. C., Jr., & Hodge, P. W. 1989a, ApJ, 347, 875
Skillman, E. D., Terlevich, R. J., Kennicutt, R. C., Jr., Garnett, D. R., & Terlevich, E. 1994, ApJ, 431, 172
Skillman, E. D., Terlevich, R., & Melnick, J. 1989b, MNRAS, 240, 563
Smith, H. E. 1975, ApJ, 199, 591
Terlevich, R., Melnick, J., Masegosa, J., Moles, M., & Copetti, V. F. 1991, A&AS, 91, 285
Thuan, T. X., Izotov, Y. I., & Foltz, C. B. 1999, ApJ, 525, 105
Thuan, T. X., Izotov, Y. I., & Lipovetsky, V. A. 1995, ApJ, 445, 108
Torres-Peimbert, S., Peimbert, M., & Fierro, J. 1989, ApJ, 345, 186
Tsamis, Y. G., Barlow, M. J., Liu, X.-W., Danziger, I. J., & Storey, P. J. 2003, MNRAS, 338, 687
Tully, R. B., Boesgaard, A. M., Dyck, H. M., & Schempp, W. V. 1981, ApJ, 246, 38
van Zee, L. 2000, ApJ, 543, L31
van Zee, L., Haynes, M. P., & Salzer, J. J. 1997, AJ, 114, 2479
van Zee, L., Salzer, J. J., Haynes, M. P., O'Donoghue, A. A., & Balonek, T. J. 1998, AJ, 116, 2805
Vermeij, R., Damour, F., van der Hulst, J. M., & Baluteau, J.-P. 2002, A&A, 390, 649
Vílchez, J. M., & Iglesias-Páramo, J. 1998, ApJ, 508, 248
———. 2003, ApJS, 145, 225
Vílchez, J. M., Pagel, B. E. J., Díaz, A. I., Terlevich, E., & Edmunds, M. G. 1988, MNRAS, 235, 633
Webster, B. L., Longmore, A. J., Hawarden, T. G., & Mebold, U. 1983, MNRAS, 205, 643
Webster, B. L., & Smith, M. G. 1983, MNRAS, 204, 743
Zaritsky, D., Kennicutt, R. C., Jr., & Huchra, J. P. 1994, ApJ, 420, 87
Zasov, A. V., Kniazev, A. Y., Pustilnik, S. A., Pramsky, A. G., Burenkov, A. N., Ugryumov, A. V., & Martin, J.-M. 2000, A&AS, 144, 429